Journal of Materials Chemistry A

ROYAL SOCIETY OF CHEMISTRY

COMMUNICATION

View Article Online
View Journal | View Issue

Cite this: J. Mater. Chem. A, 2024, 12, 2680

Received 20th December 2023
Accepted 9th January 2024

DOI: 10.1039/d3ta07898a

rsc.li/materials-a

Three-dimensional porous NiCoP foam enabled high-performance overall seawater splitting at high current density†

Li He,[a] Zhengwei Cai,[b] Dongdong Zheng,[b] Ling Ouyang,[a] Xun He,[a] Jie Chen,[a] Ye Li,[a] Xiankun Guo,[a] Qian Liu,[c] Luming Li,[c] Wei Chu,[c] Shuyun Zhu,*[d] Xuping Sun*[ab] and Bo Tang*[be]

Developing high-performance bifunctional electrocatalysts for hydrogen and oxygen evolution reactions (HER and OER) is essential to future renewable energy systems. Herein, a three-dimensional (3D) porous NiCoP foam on Ni foam (NiCoP foam/NF) is designed and employed as an outstanding bifunctional electrocatalyst for overall seawater splitting, requiring only 328 mV and 356 mV overpotentials for the HER and OER, respectively, at an industrial-level current density of 1000 mA cm^{-2}. Moreover, the 3D NiCoP foam/NF-assembled two-electrode electrolyzer can operate at a low cell voltage of 1.97 V to obtain 1000 mA cm^{-2} and present a stable response for over 300 h in alkaline seawater, underscoring its potential for sustainable energy applications.

Hydrogen (H_2), recognized as a highly promising alternative to traditional fuels, stands out due to its high energy density (142 MJ kg^{-1}) and environmentally friendly nature.[1,2] Electrochemical water splitting, involving an anodic oxygen evolution reaction (OER) and a cathodic hydrogen evolution reaction (HER), offers a green and efficient approach to producing sustainable H_2.[3–7] Particularly, given the abundant availability of seawater on earth, direct electrolysis of seawater has garnered increasing attention for large-scale H_2 production, but the high concentrations of the chloride anion (Cl^-) in seawater can lead to the undesirable chloride evolution reaction competing with anodic OER and even continuously corrode the electrode, which greatly restricts the development of seawater splitting technology.[8–17] Using a bifunctional water-splitting electrocatalyst operating efficiently for both the OER and HER has advantages of simplifying the system and lowering the cost.[18] As such, it is of great importance to develop high-activity, robust, and non-precious bifunctional electrocatalysts for overall seawater splitting in the same electrolyte.[19,20]

In this context, there has been a surge in research to explore earth-abundant transition metal-based materials as cost-effective bifunctional electrocatalysts for electrocatalytic seawater splitting, including oxides,[21,22] hydroxides,[23,24] sulfides,[19] phosphides,[25,26] nitrides,[27] *etc.* In particular, transition metal phosphides (TMPs) with excellent catalytic activity and good corrosion resistance have been widely reported as efficient bifunctional electrocatalysts for overall seawater splitting, for instance, Mo–CoP_x,[28] Fe–Ni_2P,[29] and Co–Fe_2P.[30] Significantly, the negatively charged P in TMPs enhances water molecule splitting into H* or OH*, and optimizes the free energy of adsorbed hydrogen atoms, thus boosting the catalytic efficiency.[31,32] Simultaneously, the phosphate anion obtained by the oxidation of P can impose a repulsive effect on Cl^-, thus averting the corrosion of the electrode by Cl^-, further enhancing the material's durability.[33] In addition, both theoretical and experimental results have shown that the enhanced catalytic activity of TMPs can be achieved by the introduction of additional metal atoms, for the electronic regulation and synergistic effects, so bimetallic ternary phosphides usually show better catalytic performance than the counterpart single metal binary phosphides.[34,35]

Herein, we employ NiCoP foam on Ni foam (NiCoP foam/NF) as a superb bifunctional electrocatalyst for overall seawater splitting, using the dynamic hydrogen bubble template (DHBT) method followed by phosphidation. Remarkably, the resulting NiCoP foam/NF catalyst, with its unique three-dimensional (3D) porous structure, exhibits excellent electrocatalytic activity. It achieves low overpotentials of just 328 mV for the HER and 356 mV for the OER at a high current density (*j*) of 1000 mA cm^{-2}. Moreover, the 3D NiCoP foam/NF-assembled two-electrode electrolyzer can operate at a low cell voltage of

[a]Institute of Fundamental and Frontier Sciences, University of Electronic Science and Technology of China, Chengdu 610054, Sichuan, China. E-mail: xpsun@uestc.edu.cn; xpsun@sdnu.edu.cn

[b]College of Chemistry, Chemical Engineering and Materials Science, Shandong Normal University, Jinan 250014, Shandong, China. E-mail: tangb@sdnu.edu.cn

[c]Institute for Advanced Study, Chengdu University, Chengdu 610106, Sichuan, China

[d]College of Chemistry and Chemical Engineering, Qufu Normal University, Qufu 273165, Shandong, China. E-mail: shuyunzhu1981@163.com

[e]Laoshan Laboratory, Qingdao 266237, Shandong, China

† Electronic supplementary information (ESI) available: Experimental section and supplementary figures. See DOI: https://doi.org/10.1039/d3ta07898a

1.97 V at 1000 mA cm^{-2} and present a stable response for over 300 h in alkaline seawater, outperforming most recently reported electrocatalysts.

The 3D self-supported NiCoP foam, characterized by its highly porous structure, was synthesized as depicted in Fig. 1a (see the ESI† for more preparative details). The crystalline phase composition of the NiCoP foam/NF was characterized by X-ray diffraction (XRD). As displayed in Fig. 1b, the XRD pattern presents diffraction peaks that match well with a NiCoP crystal phase (PDF No. 71-2336) and metallic Ni (PDF No. 70-1849). The scanning electron microscopy (SEM) images of NiCoP foam/NF (Fig. 1c) suggest full coverage of the porous structure on nickel foam (Fig. S1†). Notably, the pore side walls were formed from more "loosely" packed NiCoP clusters, together like a cauliflower (Fig. 1c inset), leading to a secondary porosity on the nanoscale. The SEM and corresponding energy-dispersive X-ray (EDX) elemental mapping images (Fig. 1d) show a uniform distribution of Co, Ni, and P elements, suggesting the successful preparation of phosphides. The high-resolution transmission electron microscopy (HRTEM) image (Fig. 1e) displays a lattice spacing of 0.23 nm assigned to the (111) lattice plane of NiCoP.[36] Additionally, the Co_2P foam/NF (Fig. S2†) and Ni_2P foam/NF (Fig. S3†) counterparts were also fabricated and characterized for comparison. The surface chemical state of the NiCoP foam/NF can be determined by X-ray photoelectron spectroscopy (XPS). In the Co $2p_{3/2}$ core-level spectrum (Fig. S4a†), three distinct peaks are observed: a satellite peak at 785.9 eV, a peak for oxidized Co–PO_x (Co^{2+}) at 781.2 eV, and a peak at 778.2 eV corresponding to the partially charged Co species ($Co^{\delta+}$, δ is likely close to 0) caused by Co–P bonds. The Co $2p_{1/2}$ region, characterized by peaks at 792.7, 797.6, and 802.8 eV, is associated with Co–P, oxidized Co species, and the satellite, respectively.[37,38] The Ni $2p_{3/2}$ spectrum (Fig. S4b†) reveals three peaks at binding energies of 852.6, 856.1, and 860.8 eV, corresponding to partially charged Ni–P species ($Ni^{\delta+}$, δ is likely close to 0), oxidized Ni–PO_x (Ni^{2+}), and the satellite peak, respectively.[39] Additionally, the Ni $2p_{1/2}$ region exhibits two peaks at 869.7 eV (Ni–P) and 873.8 eV (oxidized Ni species), and one satellite peak at 879.3 eV.[39] In the P 2p XPS spectrum (Fig. S4c†), the two peaks at 129.0 and 130.1 eV are indicative of P $2p_{1/2}$ and P $2p_{3/2}$, respectively, while the broad feature near around 133.0 eV is attributed to the phosphate species (P–O).[40]

The electrochemical HER activity of the catalysts was evaluated in a strong alkaline seawater environment (1 M KOH + seawater). Fig. 2a displays the linear sweep voltammetry (LSV) curves of NiCoP foam/NF, Co_2P foam/NF, Ni_2P foam/NF, the benchmark Pt/C/NF, and blank NF. The NiCoP foam/NF can drive the current densities of 100, 500, and 1000 mA cm^{-2} at notably lower overpotentials of 171, 262, and 328 mV, respectively (Fig. 2b), which are superior to the counterparts of Co_2P foam/NF (221, 313, and 390 mV, respectively), Ni_2P foam/NF (233, 430, and 600 mV, respectively), Pt/C/NF (279, 384, and 493 mV, respectively), and blank NF (222, 462, and 688 mV, respectively). Moreover, the required overpotential of just

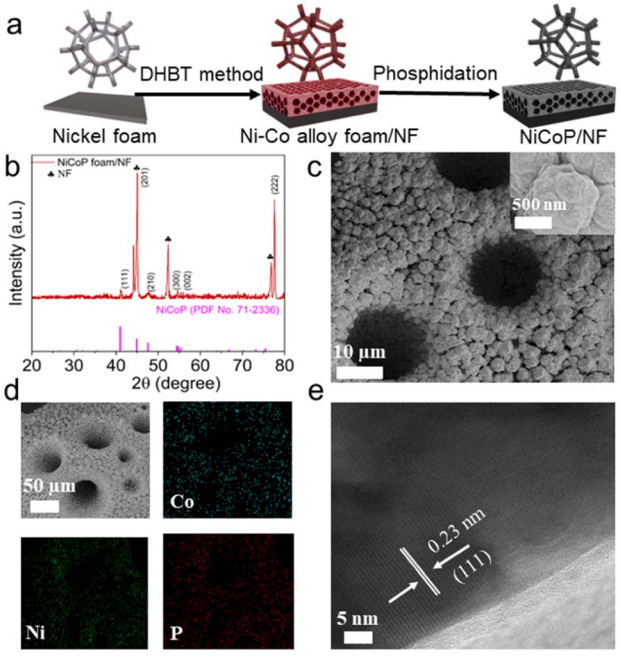

Fig. 1 Synthesis and structural analysis of NiCoP foam/NF. (a) Schematic illustration of the fabrication procedure of NiCoP foam/NF. (b) XRD pattern of NiCoP foam/NF. (c) SEM images of NiCoP foam/NF. (d) SEM and the corresponding EDX elemental mapping images of NiCoP foam/NF. (e) HRTEM image of the NiCoP.

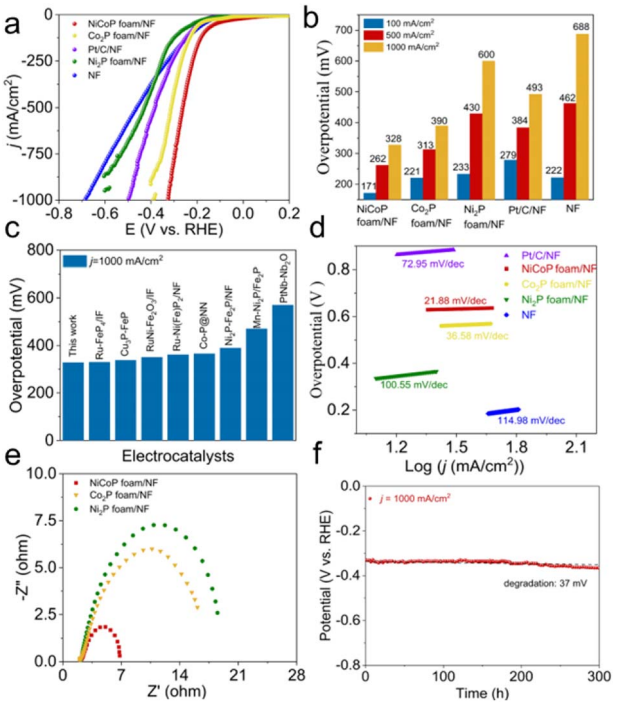

Fig. 2 Hydrogen evolution catalysis. (a) LSV curves and (b) the overpotentials for different electrocatalysts in 1 M KOH + seawater. (c) Comparison of overpotentials required to achieve a j of 1000 mA cm^{-2} between NiCoP foam/NF and other self-supported catalysts in alkaline seawater. (d) Tafel plots of different electrocatalysts in 1 M KOH + seawater. (e) Nyquist plots of NiCoP foam/NF, Co_2P foam/NF, and Ni_2P foam/NF in 1 M KOH + seawater. (f) Chronopotentiometry testing of NiCoP foam/NF at a j of 1000 mA cm^{-2} in alkaline seawater.

328 mV at 1000 mA cm^{-2} is competitive with most reported HER electrocatalysts in alkaline seawater, as detailed in Fig. 2c and Table S1.† The Tafel slope is a key parameter to illustrate the kinetic information of the catalysts. Remarkably, the NiCoP foam/NF exhibits a Tafel slope of 21.88 mV dec^{-1} (Fig. 2d), significantly lower than those of Co_2P foam/NF (36.58 mV dec^{-1}), Ni_2P foam/NF (100.55 mV dec^{-1}), Pt/C/NF (72.95 mV dec^{-1}), and blank NF (114.98 mV dec^{-1}), which demonstrates the fastest HER kinetics of NiCoP foam/NF. Electrochemical impedance spectroscopy (EIS) further revealed enhanced reaction kinetics and charge transfer capabilities in NiCoP foam/NF, evidenced by a lower charge transfer resistance compared to Co_2P foam/NF and Ni_2P foam/NF (Fig. 2e). Cyclic voltammetry curves were used to calculate the double-layer capacitance (C_{dl}), which is dependent on the electrochemically active surface area. The C_{dl} of NiCoP foam/NF was measured at 12.55 mF cm^{-2} (Fig. S5†), higher than those of Co_2P foam/NF (9.16 mF cm^{-2}) and Ni_2P foam/NF (2.65 mF cm^{-2}), confirming the larger electrochemically active surface area of NiCoP foam/NF, thereby enhancing its HER catalysis capabilities compared to other foams. The multi-current step chronopotentiometry curve (Fig. S6†) shows rapid potential stabilization at each step, indicating the remarkable mass transport capability of NiCoP foam/NF for the HER. Long-term stability is a crucial factor for industrial seawater electrolysis due to its direct impact on the lifespan of the catalyst and, consequently, the cost of hydrogen production. To this end, the electrochemical HER stability test of NiCoP foam/NF was conducted at a high j of 1000 mA cm^{-2} in alkaline seawater over 300 h (Fig. 2f). The potential remained almost constant with a minimal degradation of 37 mV. Furthermore, the SEM images (presented in Fig. S7†) and XRD pattern (shown in Fig. S8†) of NiCoP foam/NF reveal that the 3D porous structure and the crystalline phase of the material are well preserved after the HER stability test.

The electrocatalytic OER activity of NiCoP foam/NF, Co_2P foam/NF, Ni_2P foam/NF, RuO_2/NF, and blank NF was tested in alkaline seawater, and the related LSV curves are shown in Fig. 3a. Mirroring the HER results, NiCoP foam/NF demonstrates the highest catalytic activity among these catalysts. Specifically, the NiCoP foam/NF requires an overpotential of only 291 mV to achieve 100 mA cm^{-2}, which is significantly lower than those of Co_2P foam/NF (337 mV), Ni_2P foam/NF (423 mV), RuO_2/NF (453 mV), and NF (518 mV), as shown in Fig. 3b. Ni_2P foam/NF, RuO_2/NF, and NF are incapable of reaching a high j of 1000 mA cm^{-2} in the applied potential range. For NiCoP foam/NF, the overpotential required to achieve 1000 mA cm^{-2} (η_{1000}) is only 356 mV, whereas η_{1000} of 537 mV is obtained for Co_2P foam/NF, reflecting the excellent OER activity of NiCoP foam/NF. Furthermore, the excellent catalytic activity (η_{1000}) of NiCoP foam/NF is competitive with most reported OER electrocatalysts in alkaline seawater, as detailed in Fig. 3c and Table S2.† The OER kinetics of these catalysts are further assessed through Tafel slope analysis, presented in Fig. 3d. The Tafel slopes of NiCoP foam/NF, Co_2P foam/NF, Ni_2P foam/NF, RuO_2/NF, and NF are 17.87, 29.47, 72.83, 91.24, and 128.25 mV dec^{-1}, respectively, indicating the more favorable OER kinetics of NiCoP foam/NF. Additionally, the multi-current step

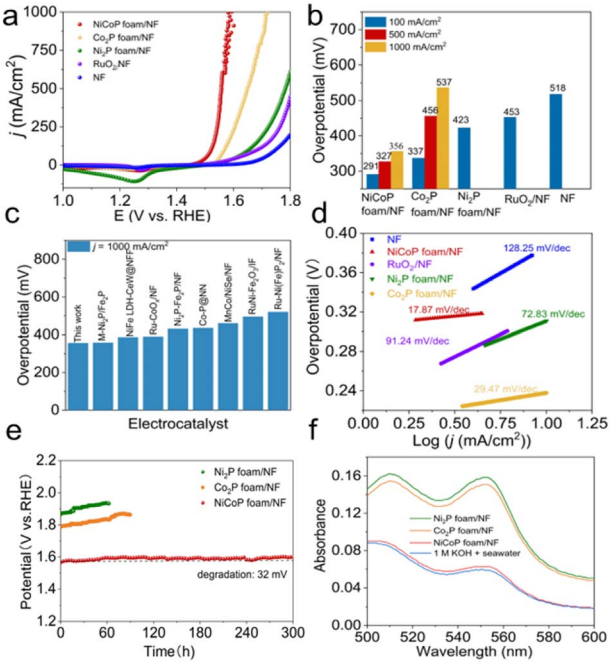

Fig. 3 Oxygen evolution catalysis. (a) LSV curves and (b) comparison of the overpotentials for different electrocatalysts in 1 M KOH + seawater. (c) Comparison of overpotentials at 1000 mA cm^{-2} for NiCoP foam/NF and other electrocatalysts in alkaline seawater. (d) Tafel plots of different electrocatalysts in 1 M KOH + seawater. (e) Chronopotentiometry testing of Ni_2P foam/NF, Co_2P foam/NF, and NiCoP foam/NF at a j of 1000 mA cm^{-2} in 1 M KOH + seawater electrolyte at room temperature. (f) UV-vis absorption spectra of electrolysis following an electrolysis durability test for NiCoP foam/NF, Co_2P foam/NF, and Ni_2P foam/NF at a j of 1000 mA cm^{-2} in 1 M KOH + seawater.

chronopotentiometry curve for the OER (Fig. S9†) corroborates the remarkable mass transport capability of NiCoP foam/NF. Moreover, NiCoP foam/NF also exhibits exceptional long-term stability in the electrocatalytic OER process. Furthermore, NiCoP foam/NF exhibits remarkable stability when tested at a current density of 1000 mA cm^{-2} in alkaline seawater over 300 h, showing only a minor potential degradation of 32 mV. In stark contrast, its counterparts, Co_2P foam/NF and Ni_2P foam/NF, display inferior performance and lack stability under similar conditions (Fig. 3e). Further evidence of NiCoP foam/NF's superior stability is provided by UV-vis spectrophotometer results (Fig. 3f and S10†), which indicate a negligible generation of hypochlorite (ClO^-) compared to the significant ClO^- generation observed in both Co_2P foam/NF and Ni_2P foam/NF, highlighting the superior corrosion resistance and high selectivity of NiCoP foam/NF in seawater oxidation. Additionally, the SEM images of NiCoP foam/NF following the OER durability test (Fig. S11†) demonstrate that its 3D porous structure remained well preserved. Remarkably, the XRD pattern (Fig. S12†) shows that the diffraction peaks are consistent with those of the initial catalyst. Meanwhile, the HRTEM image in Fig. S13† reveals an amorphous oxyhydroxide layer on the surface of NiCoP, identified as the active center for the OER.[40,41] This presence of oxyhydroxide is then further substantiated by the XPS Ni 2p and

Co 2p spectra, indicating an elevated valence state of Ni and Co following the reaction. Additionally, a diminished intensity of the P 2p is observed in Fig. S14c,† where only the broad phosphorus PO_4^{3-} is detected. PO_4^{3-} is thought to play a crucial role in repelling Cl^- in seawater during the OER test.[42,43]

In light of the remarkable HER and OER performance catalyzed by NiCoP foam/NF, a self-assembled electrolyzer employing NiCoP foam/NF as both the anode and cathode was constructed to investigate overall alkaline seawater electrolysis (shown in Fig. 4a). The NiCoP foam/NF-assembled two electrode electrolyzer performs better than the benchmark RuO_2/NF||Pt/C/NF (Fig. 4b). NiCoP foam/NF||NiCoP foam/NF requires cell voltages of only 1.28, 1.68, and 1.97 V to achieve current densities of 100, 500, and 1000 mA cm^{-2}, respectively, which are notably lower than the voltages obtained for the RuO_2/NF||Pt/C/NF with 1.90, 2.39, and 2.80 V, respectively (as shown in Fig. 4c). Additionally, the electrolyzer retains its excellent performance over 300 h of steady electrolysis at a j of 1000 mA cm^{-2} in alkaline seawater (Fig. 4d). The excellent performance, coupled with its durability, positions the NiCoP foam/NF-assembled two-electrode electrolyzer favorably against the most recently reported bifunctional electrocatalysts in alkaline seawater (as detailed in Table S3†), which underscores the potential of NiCoP foam/NF as a highly efficient and durable catalyst, offering significant promise for sustainable seawater electrolysis applications. The remarkable performance of NiCoP foam/NF in seawater splitting can be attributed to several key factors: (1) its 3D porous structure creates more channels for mass transfer and enables the rapid detachment of bubbles. (2) The synergistic effects of Ni and Co in NiCoP facilitate efficient HER. (3) The *in situ* formation of oxyhydroxides during seawater oxidation serves as active sites for the reaction. (4) The generation of PO_4^{3-} from the oxidation of P during the OER test helps counteract the effects of Cl^-.

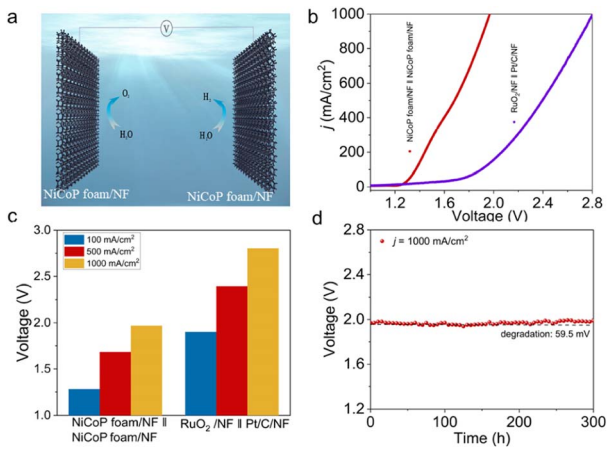

Fig. 4 Overall seawater splitting performance. (a) Schematic illustration of the overall seawater splitting system. (b) Polarization curves of NiCoP foam/NF||NiCoP foam/NF and RuO_2/NF||Pt/C/NF in alkaline seawater. (c) Comparison of the voltages at different current densities between NiCoP foam/NF||NiCoP foam/NF and RuO_2/NF||Pt/C/NF in alkaline seawater. (d) Chronopotentiometry testing of NiCoP foam/NF||NiCoP foam/NF at a j of 1000 mA cm^{-2} in alkaline seawater.

In conclusion, NiCoP foam/NF, with its 3D porous structure, demonstrates high efficiency and robustness as a bifunctional electrocatalyst in alkaline seawater for overall seawater splitting. It achieves low overpotentials of 328 mV for the HER and 356 mV for the OER at an industrial-level current density of 1000 mA cm^{-2}. Notably, the two-electrode seawater electrolyzer employing NiCoP foam/NF as both the anode and cathode consistently delivers 1000 mA cm^{-2} at a cell voltage of 1.97 for over 300 h. Our work not only provides an efficient bifunctional electrocatalyst for overall seawater splitting but also opens avenues for further exploration of bimetallic ternary phosphides for applications.

Conflicts of interest

There are no conflicts to declare.

Acknowledgements

This work was supported by the Free Exploration Project of Frontier Technology for Laoshan Laboratory (No. 16-02) and the National Natural Science Foundation of China (No. 22072015 and 21927811).

References

1 Z. W. Seh, J. Kibsgaard, C. F. Dickens, I. Chorkendorff, J. K. Nørskov and T. F. Jaramillo, *Science*, 2017, **355**, eaad4998Y.
2 H. Jin, X. Wang, C. Tang, A. Vasileff, L. Li, A. Slattery and S. Z. Qiao, *Adv. Mater.*, 2021, **33**, 2007508.
3 B. Wu, S. Gong, Y. Lin, T. Li, A. Chen, M. Zhao, Q. Zhang and L. Chen, *Adv. Mater.*, 2022, **34**, 2108619.
4 J. Wang, Q. Liu, W. Cui, Z. Xing, A. M. Asiri and X. Sun, *Adv. Mater.*, 2016, **28**, 215–230.
5 P. M. Bodhankar, P. B. Sarawade, G. Singh, A. Vinu and D. S. Dhwale, *J. Mater. Chem. A*, 2021, **9**, 3180–3208.
6 Q. Wu, Q. Gao, X. Wang, Y. Qi, L. Shen, X. Tai, F. Yang, X. He, Y. Wang, Y. Yao, Y. Ren, Y. Luo, S. Sun, D. Zheng, Q. Liu, S. Alfaifi, X. Sun and B. Tang, *iScience*, 2024, **27**, 108738.
7 H. Zhang, H. Han, X. Yang, H. Ma, Z. Song and X. Ji, *Catal. Sci. Technol.*, 2023, **13**, 6951–6958.
8 Z. Chen, Q. Li, H. Xiang, Y. Wang, P. Yang, C. Dai, H. Zhang, W. Xiao, Z. Wu and L. Wang, *Inorg. Chem. Front.*, 2023, **10**, 1493–1500.
9 X. Wang, M. Geng, S. Sun, Q. Xiang, S. Dong, K. Dong, Y. Yao, Y. Wang, Y. Yang, Y. Luo, D. Zheng, Q. Liu, J. Hu, Q. Wu, X. Sun and B. Tang, *J. Mater. Chem. A*, 2024, **12**, 634–656.
10 X. Wu, S. Zhou, Z. Wang, J. Liu, W. Pei, P. Yang, J. Zhao and J. Qiu, *Adv. Energy Mater.*, 2019, **9**, 1901333.
11 J. Liang, Z. Li, X. He, Y. Luo, D. Zheng, Y. Wang, T. Li, B. Ying, S. Sun, Z. Cai, Q. Liu, B. Tang and X. Sun, *Mater. Today*, 2023, **69**, 193–235.
12 L. Yu, Q. Zhu, S. Song, B. McElhenny, D. Wang, C. Wu, Z. Qiu, J. Bao, Y. Yu, S. Chen and Z. Ren, *Nat. Commun.*, 2019, **10**, 5106.

13 Y. Yao, C. Yang, S. Sun, H. Zhang, M. Geng, X. He, K. Dong, Y. Luo, D. Zheng, W. Zhuang, S. Alfaifi, A. Farouk, M. S. Hamdy, B. Tang, S. Zhu and X. Sun, *Small*, 2023, DOI: **10.1002/smll.202307294**.
14 L. Wu, L. Yu, Q. Zhu, B. McElhenny, F. Zhang, C. Wu, X. Xing, J. Bao, S. Chen and Z. Ren, *Nano Energy*, 2021, **83**, 105838.
15 Z. Li, Y. Yao, S. Sun, J. Liang, S. Hong, H. Zhang, C. Yang, X. Zhang, Z. Cai, J. Li, Y. Ren, Y. Luo, D. Zheng, X. He, Q. Liu, Y. Wang, F. Gong, X. Sun and B. Tang, *Angew. Chem., Int. Ed.*, 2023, **63**, e202316522.
16 J. Tang, S. Sun, X. He, H. Zhang, C. Yang, M. Zhang, M. Yue, H. Wang, Y. Sun, Y. Luo, S. Alfaifi, A. Farouk, M. S. Hamdy, X. Sun, H. Wang and B. Ying, *Nano Res.*, 2023, DOI: **10.1007/s12274-023-6087-y**; *Nano Res.*, 2023, DOI: **10.1007/s12274-023-6002-6**.
17 H. Zhang, X. He, K. Dong, Y. Yao, S. Sun, M. Zhang, M. Yue, C. Yang, Q. Liu, Y. Luo, B. Ying, S. Alfaifi, X. Ji, B. Tang and X. Sun, *Mater. Today Phys.*, 2023, **38**, 101249.
18 C. Tang, N. Cheng, Z. Pu, W. Xing and X. Sun, *Angew. Chem., Int. Ed.*, 2015, **54**, 9351–9355.
19 J. Chen, L. Zhang, J. Li, X. He, Y. Zheng, S. Sun, X. Fang, D. Zheng, Y. Luo, Y. Wang, J. Zhang, L. Xie, Z. Cai, Y. Sun, A. A. Alshehri, Q. Kong, C. Tang and X. Sun, *J. Mater. Chem. A*, 2023, **11**, 1116–1122.
20 L. Wu, L. Yu, F. Zhang, B. McElhenny, D. Luo, A. Karim, S. Chen and Z. Ren, *Adv. Funct. Mater.*, 2021, **31**, 2006484.
21 Y. Chen, X. Zhao, Q. Zhang, X. Miao, Y. Chen, W. Yang and Q. Pan, *Int. J. Hydrogen Energy*, 2023, **48**, 3759–3767.
22 J. D. Rodney, S. Deepapriya, M. C. Robinson, S. J. Das, S. Perumal, P. Sivakumar, H. Jung, B. C. Kim and C. J. Raj, *Appl. Mater. Today*, 2021, **24**, 101079.
23 K. Jiang, W. Liu, W. Lai, M. Wang, Q. Li, Z. Wang, J. Yuan, Y. Deng, J. Bao and H. Ji, *Inorg. Chem.*, 2021, **60**, 17371–17378.
24 X. Gao, J. Chen, Y. Yu, F. Wang, X. Wu, X. Wang, W. Mao, J. Li, W. Huang, Q. Chen, R. Li, C. You, S. Wang, X. Tian and Z. Kang, *Chem. Eng. J.*, 2023, **474**, 145568.
25 J. Zhu, J. Chi, T. Cui, L. Guo, S. Wu, B. Li, J. Lai and L. Wang, *Appl. Catal., B*, 2023, **328**, 122487.
26 Y. Yang, R. Zou, J. Gan, Y. Wei, Z. Chen, X. Li, S. Admassie, Y. Liu and X. Peng, *Green Chem.*, 2023, **25**, 4104–4112.
27 X. Wang, X. Han, R. Du, C. Xing, X. Qi, Z. Liang, P. Guardia, J. Arbiol, A. Cabot and J. Li, *ACS Appl. Mater. Interfaces*, 2022, **14**, 41924–41933.
28 Y. Yu, J. Luo, Z. Kang, C. Jia, Z. Liu, W. Huang, Q. Chen, P. Deng, Y. Shen and X. Tian, *Mater. Today Nano*, 2022, **18**, 100216.
29 X. Liu, Q. Yu, X. Qu, X. Wang, J. Chi and L. Wang, *Adv. Mater.*, 2024, **36**(1), 2307395.
30 S. Wang, P. Yang, X. Sun, H. Xing, J. Hu, P. Chen, Z. Cui, W. Zhu and Z. Ma, *Appl. Catal., B*, 2021, **297**, 120386.
31 Y. Shi, M. Li, Y. Yu and B. Zhang, *Energy Environ. Sci.*, 2020, **13**, 4564–4582.
32 J. Liu, X. Liu, H. Shi, J. Luo, L. Wang, J. Liang, S. Li, L. Yang, T. Wang, Y. Huang and Q. Li, *Appl. Catal., B*, 2022, **302**, 120862.
33 J. Li, Y. Hu, X. Huang, Y. Zhu and D. Wang, *Small*, 2023, **19**, 2206533.
34 R. Li, B. Wang, T. Gao, R. Zhang, C. Xu, X. Jiang, J. Zeng, Y. Bando, P. Hu, Y. Li and X. Wang, *Nano Energy*, 2019, **58**, 870–876.
35 C. Tang, R. Zhang, W. Lu, L. He, X. Jiang, A. M. Asiri and X. Sun, *Adv. Mater.*, 2017, **29**, 1602441.
36 H. S. Hu, Y. Li, Y. Shao, K. Li, G. Deng, C. Wang and Y. Feng, *J. Power Sources*, 2021, **484**, 229269.
37 X. He, Z. Li, J. Yao, K. Dong, X. Li, L. Hu, S. Sun, Z. Cai, D. Zheng, Y. Luo, B. Ying, M. S. Hamdy, L. Xie, Q. Liu and X. Sun, *iScience*, 2023, **26**, 107100.
38 J. Wang, W. Hua, M. Li, H. Liu, M. Shao and B. Wei, *ACS Appl. Mater. Interfaces*, 2018, **10**, 41237–41245.
39 C. Du, L. Yang, F. Yang, G. Cheng and W. Luo, *ACS Catal.*, 2017, **7**, 4131–4137.
40 H. Liang, A. N. Gandi, D. H. Anjum, X. Wang, U. Schwingenschlögl and H. N. Alshareef, *Nano Lett.*, 2016, **16**, 7718–7725.
41 W. Zou, C. Sun, K. Zhao, J. Li, X. Pan, D. Ye, Y. Xie, W. Xu, H. Zhao, L. Zhang and J. Zhang, *Electrochim. Acta*, 2020, **345**, 136114.
42 S. C. Sekhar, B. Ramulu, M.-H. Han, M. Nagaraju, S. J. Arbaz, H.-S. Oh and J. S. Yu, *ACS Sustainable Chem. Eng.*, 2022, **10**(43), 14163–14173.
43 T. Li, X. Zhao, M. G. Sendeku, X. Zhang, L. Xu, Z. Wang, S. Wang, X. Duan, H. Liu, W. Liu, D. Zhou, H. Xu, Y. Kuang and X. Sun, *Chem. Eng. J.*, 2023, **460**, 141413.

